Introduction

Panorama

Finslerian eikonal

Semi-Lagrangian schemes

Adaptive stencil refinement

Image segmentation

Riemannian eikonal

Monotony and causality

Grid-adapted tensor decomposition

Curvature penalization

Reeds-Shepp

Other models

Conclusion

Fast marching methods for anisotropic eikonal equations.

Jean-Marie Mirebeau

University Paris Sud, CNRS, University Paris-Saclay

April 2, 2019

Geometric processing workshop, IPAM, UCLA

In collaboration with : L. Cohen, R. Duits, Da Chen.

Introduction: anisotropy and cartesian grids

Problems addressed

Finslerian eikonal equations, and the Stern-Brocot tree
- Semi-Lagrangian schemes
- Adaptive stencil refinement
- Application to image segmentation

Riemannian eikonal equations, and Voronoi's reduction
- Monotone and causal schemes
- Grid-adapted tensor decomposition

Global optimization of curvature dependent energies
- The Reeds-Shepp models
- Euler-Mumford elastica curves, and others

Conclusion

Introduction: anisotropy and cartesian grids

Problems addressed

Finslerian eikonal equations, and the Stern-Brocot tree
- Semi-Lagrangian schemes
- Adaptive stencil refinement
- Application to image segmentation

Riemannian eikonal equations, and Voronoi's reduction
- Monotone and causal schemes
- Grid-adapted tensor decomposition

Global optimization of curvature dependent energies
- The Reeds-Shepp models
- Euler-Mumford elastica curves, and others

Conclusion

Anisotropy in Partial Differential Equations (PDEs)

Anisotropy is the existence of preferred directions, locally, in a domain. The phenomenon is generic and ubiquitous, and may have a variety of causes, such as:

- Micro-structure, either biological, geologic, synthetic.
- Different nature of the domain dimensions, e.g. $\mathbb{R}^2 \times \mathbb{S}^1$.
- Proximity of the domain boundary, or of discontinuities.

Anisotropy in Partial Differential Equations (PDEs)

Anisotropy is the existence of preferred directions, locally, in a domain. The phenomenon is generic and ubiquitous, and may have a variety of causes, such as:

- Micro-structure, either biological, geologic, synthetic.
- Different nature of the domain dimensions, e.g. $\mathbb{R}^2 \times \mathbb{S}^1$.
- Proximity of the domain boundary, or of discontinuities.

In the numerical analysis of PDEs, (strong) anisotropy is a source of difficulties.

- Increased numerical cost, accuracy loss, instabilities or failure of the numerical methods.

Several approaches can be envisioned to address these.

First approach: adapt the domain representation

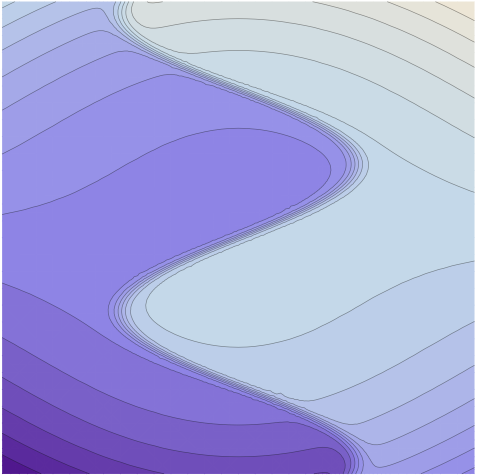

Figure: Adaptive interpolation of a function with a sharp transition.

First approach: adapt the domain representation

- Encode the problem anisotropy in a Riemannian metric.

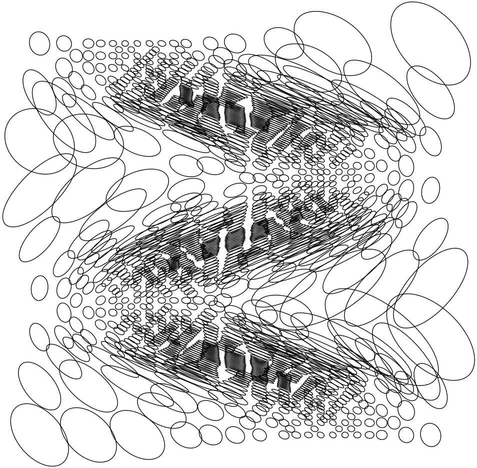

Figure: Adaptive interpolation of a function with a sharp transition.

First approach: adapt the domain representation

- Encode the problem anisotropy in a Riemannian metric.
- Create an anisotropic mesh of the domain.

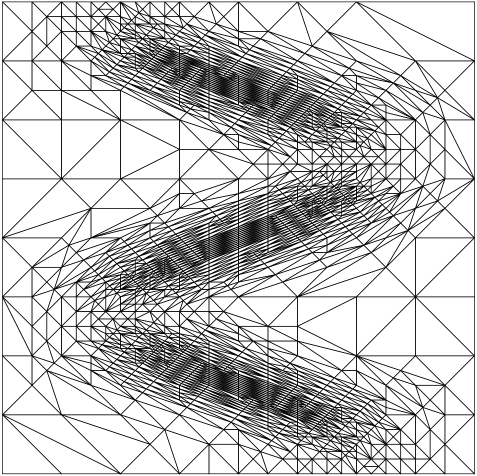

Figure: Adaptive interpolation of a function with a sharp transition.

Introduction

Panorama

Finslerian eikonal

Semi-Lagrangian schemes

Adaptive stencil refinement

Image segmentation

Riemannian eikonal

Monotony and causality

Grid-adapted tensor decomposition

Curvature penalization

Reeds-Shepp

Other models

Conclusion

Second approach: adapt the numerical scheme

- A basic cartesian grid is used throughout this work.

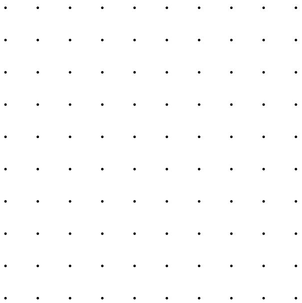

- Easily address asymmetric or three dimensional anisotropy.

Second approach: adapt the numerical scheme

- A basic cartesian grid is used throughout this work.

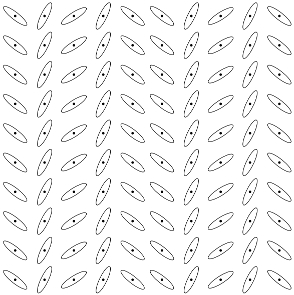

- Easily address asymmetric or three dimensional anisotropy.

Second approach: adapt the numerical scheme

- A basic cartesian grid is used throughout this work.
- Local adaptive stencils are created independently at each point, without any consistency constraint.

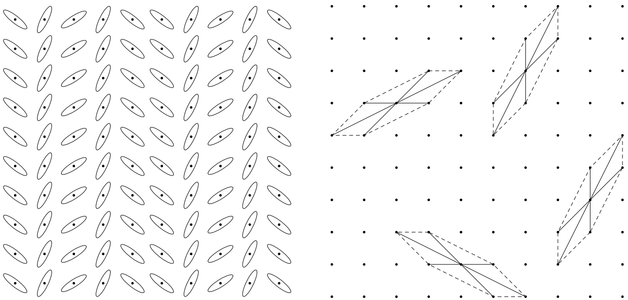

- Easily address asymmetric or three dimensional anisotropy.

Second approach: adapt the numerical scheme

- A basic cartesian grid is used throughout this work.
- Local adaptive stencils are created independently at each point, without any consistency constraint.

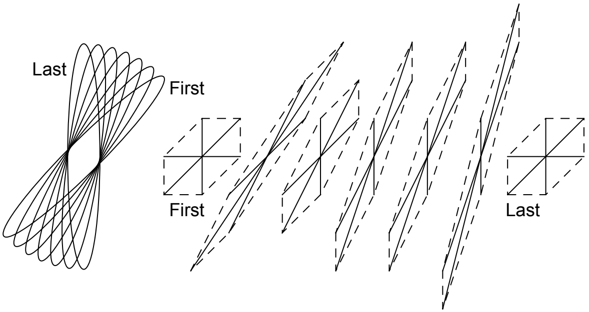

- Easily address asymmetric or three dimensional anisotropy.

Second approach: adapt the numerical scheme

- A basic cartesian grid is used throughout this work.
- Local adaptive stencils are created independently at each point, without any consistency constraint.

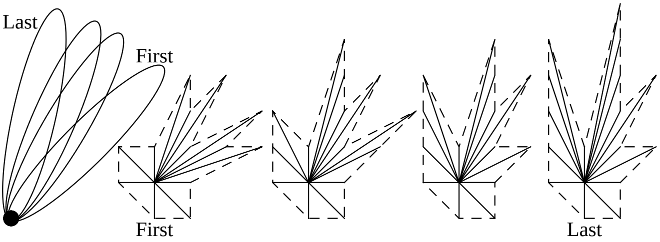

- Easily address asymmetric or three dimensional anisotropy.

Second approach: adapt the numerical scheme

- A basic cartesian grid is used throughout this work.
- Local adaptive stencils are created independently at each point, without any consistency constraint.

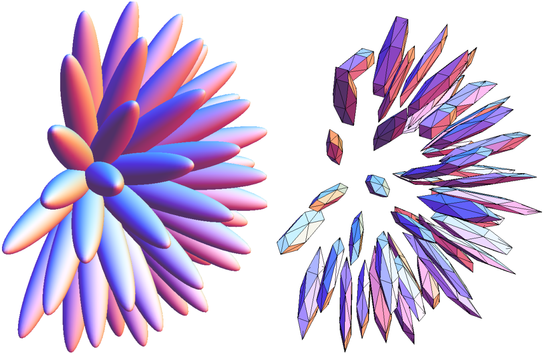

- Easily address asymmetric or three dimensional anisotropy.

Comparative advantages of the two approaches

Adaptive meshes

- Locally adjust the sampling density.
- Domains of arbitrary shape, and topology.

Different tools for different applications.

Comparative advantages of the two approaches

Adaptive meshes

- Locally adjust the sampling density.
- Domains of arbitrary shape, and topology.

Adaptive stencils on cartesian grids

- Simplicity of implementation.
- Numerical cost.
- Tools of lattice geometry.

Different tools for different applications.

Comparative advantages of the two approaches

Adaptive meshes

- Locally adjust the sampling density.
- Domains of arbitrary shape, and topology.
- Conforming meshes are a pre-requisite for some applications (e.g. finite volume or finite element schemes).

Adaptive stencils on cartesian grids

- Simplicity of implementation.
- Numerical cost.
- Tools of lattice geometry.
- Cartesian grids are a pre-requisite for some applications (e.g image processing).

Different tools for different applications.

Comparative advantages of the two approaches

Adaptive meshes

- Locally adjust the sampling density.
- Domains of arbitrary shape, and topology.
- Conforming meshes are a pre-requisite for some applications (e.g. finite volume or finite element schemes).

Adaptive stencils on cartesian grids

- Simplicity of implementation.
- Numerical cost.
- Tools of lattice geometry.
- Cartesian grids are a pre-requisite for some applications (e.g image processing).

Different tools for different applications.

Lattice geometry

Is the simultaneous study of a positive quadratic form, and of a discrete subgroup of a vector space.

Lattice geometry

Is the simultaneous study of a positive quadratic form, and of a discrete subgroup of a vector space.

Sample applications

- *What is the densest periodic packing of spheres ?*

Lattice geometry

Is the simultaneous study of a positive quadratic form, and of a discrete subgroup of a vector space.

Sample applications

- *What is the densest periodic packing of spheres ?*

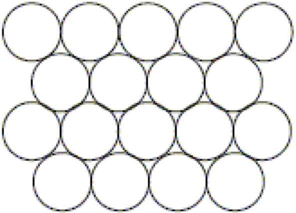

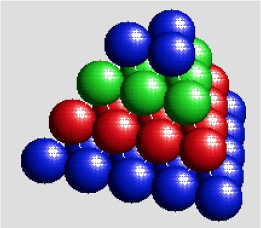

Lattice geometry

Is the simultaneous study of a positive quadratic form, and of a discrete subgroup of a vector space.

Sample applications

- *What is the densest periodic packing of spheres ?*
- *Which integers are sums of three squares ?*

Lattice geometry

Is the simultaneous study of a positive quadratic form, and of a discrete subgroup of a vector space.

Sample applications

- *What is the densest periodic packing of spheres ?*
- *Which integers are sums of three squares ?*
  Legendre's theorem:
  $$\mathbb{N} = \{i^2 + j^2 + k^2; (i,j,k) \in \mathbb{Z}^3\} \sqcup \{4^a(8b+7); a, b \in \mathbb{N}\}.$$

Lattice geometry

Is the simultaneous study of a positive quadratic form, and of a discrete subgroup of a vector space.

Sample applications

- *What is the densest periodic packing of spheres ?*
- *Which integers are sums of three squares ?*
- Message coding: error correction, cryptography.

What are the prime factors of RSA-768 ?

1230186684530117755130494958384962720772853569595334792197322452151726400507263657518745202199786469389956474942774063845925192557326303453731548268507917026122142913461670429214311602221240479274737794080665351419597459856902143413

Lattice geometry

Is the simultaneous study of a positive quadratic form, and of a discrete subgroup of a vector space.

Sample applications

- *What is the densest periodic packing of spheres ?*
- *Which integers are sums of three squares ?*
- Message coding: error correction, cryptography.

What are the prime factors of RSA-768 *?*

123018668453011775513049495838496272077285356959533479219732245215172640050726365751874520219978646938995647494277406384592519255732630345373154826850791702612214291346167042921431160222124047927473779408066535141959745985690214341 3

Conway, Sloane, *Sphere packings, lattices and groups*, 1998, has 100+ pages of references,

Lattice geometry

Is the simultaneous study of a positive quadratic form, and of a discrete subgroup of a vector space.

Sample applications

- *What is the densest periodic packing of spheres ?*
- *Which integers are sums of three squares ?*
- Message coding: error correction, cryptography.

What are the prime factors of RSA-768 *?*

1230186684530117755130494958384962720772853569595334792197322452151726400507263657518745202199786469389956474942774063845925192557326303453731548268507917026122142913461670429214311602221240479274737794080665351419597459856902143413

Conway, Sloane, *Sphere packings, lattices and groups*, 1998, has 100+ pages of references, and has been cited 6000+ times.

Introduction
Panorama
Finslerian eikonal
Semi-Lagrangian schemes
Adaptive stencil refinement
Image segmentation
Riemannian eikonal
Monotony and causality
Grid-adapted tensor decomposition
Curvature penalization
Reeds-Shepp
Other models
Conclusion

Lattice geometry

Is the simultaneous study of a positive quadratic form, and of a discrete subgroup of a vector space.

Sample applications

- *What is the densest periodic packing of spheres ?*
- *Which integers are sums of three squares ?*
- Message coding: error correction, cryptography.

What are the prime factors of RSA-768 ?

12301866845301177551304949583849627207728535695953347921973224521517264005072
63657518745202199786469389956474942774063845925192557326303453731548268507917
026122142913461670429214311602221240479274737794080665351419597459856902143413

Conway, Sloane, *Sphere packings, lattices and groups*, 1998, has 100+ pages of references, and has been cited 6000+ times.

- Few applications to PDE discretization. Bonnans et al, 04.

Introduction: anisotropy and cartesian grids

Problems addressed

Finslerian eikonal equations, and the Stern-Brocot tree
- Semi-Lagrangian schemes
- Adaptive stencil refinement
- Application to image segmentation

Riemannian eikonal equations, and Voronoi's reduction
- Monotone and causal schemes
- Grid-adapted tensor decomposition

Global optimization of curvature dependent energies
- The Reeds-Shepp models
- Euler-Mumford elastica curves, and others

Conclusion

The eikonal equation (Riemannian case)

The distance map $u : \Omega \to \mathbb{R}$ to a domain's boundary obeys

$$\|\nabla u(x)\|_{D(x)} = 1$$

for a.e. $x \in \Omega$, in viscosity sense, and $u = 0$ on $\partial\Omega$. Where $D(x)$ is the inverse metric tensor and $\|v\|_D := \sqrt{\langle v, Dv \rangle}$.

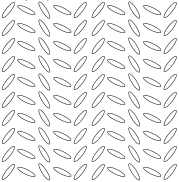

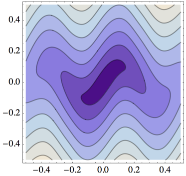

The eikonal equation (Riemannian case)

The distance map $u : \Omega \to \mathbb{R}$ to a domain's boundary obeys

$$\|\nabla u(x)\|_{D(x)} = 1$$

for a.e. $x \in \Omega$, in viscosity sense, and $u = 0$ on $\partial\Omega$. Where $D(x)$ is the inverse metric tensor and $\|v\|_D := \sqrt{\langle v, Dv\rangle}$.

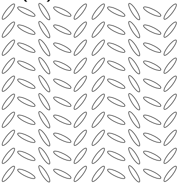

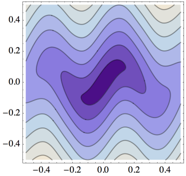

The eikonal equation (Riemannian case)

The distance map $u : \Omega \to \mathbb{R}$ to a domain's boundary obeys

$$\|\nabla u(x)\|_{D(x)} = 1$$

for a.e. $x \in \Omega$, in viscosity sense, and $u = 0$ on $\partial\Omega$. Where $D(x)$ is the inverse metric tensor and $\|v\|_D := \sqrt{\langle v, Dv \rangle}$.

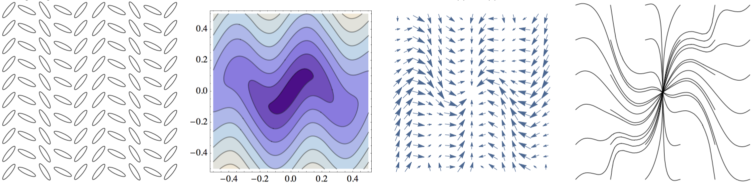

The eikonal equation (Riemannian case)

The distance map $u : \Omega \to \mathbb{R}$ to a domain's boundary obeys

$$\|\nabla u(x)\|_{D(x)} = 1$$

for a.e. $x \in \Omega$, in viscosity sense, and $u = 0$ on $\partial\Omega$. Where $D(x)$ is the inverse metric tensor and $\|v\|_D := \sqrt{\langle v, Dv \rangle}$.

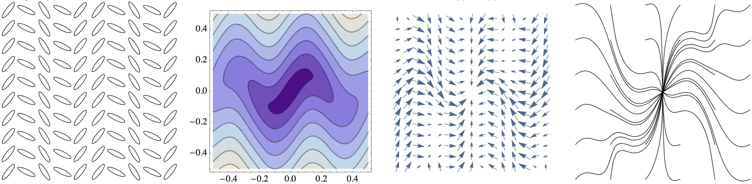

Contribution: Single pass methods for (strongly) anisotropic pb.

The eikonal equation (Riemannian case)

The distance map $u : \Omega \to \mathbb{R}$ to a domain's boundary obeys

$$\|\nabla u(x)\|_{D(x)} = 1$$

for a.e. $x \in \Omega$, in viscosity sense, and $u = 0$ on $\partial\Omega$. Where $D(x)$ is the inverse metric tensor and $\|v\|_D := \sqrt{\langle v, Dv\rangle}$.

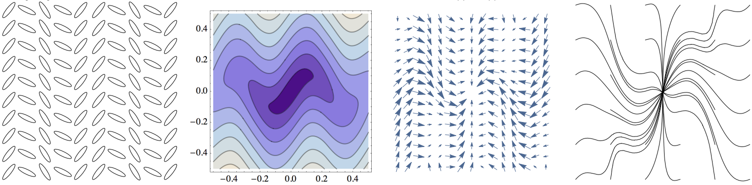

Contribution: Single pass methods for (strongly) anisotropic pb.

Applications

- Image segmentation, with L. Cohen, R. Duits, *et al*
- Motion planning, with J. Dreo (Thales).
- Perspectives: Seismology, with L. Metivier.

Anisotropic diffusion

Given a diffusion tensor field $D : \Omega \subseteq \mathbb{R}^d \to S_d^{++}$, takes the form

$$\partial_t u = \operatorname{div}(D \nabla u),$$

with suitable initial and boundary conditions.

Anisotropic diffusion

Given a diffusion tensor field $D : \Omega \subseteq \mathbb{R}^d \to S_d^{++}$, takes the form

$$\partial_t u = \operatorname{div}(D \nabla u),$$

with suitable initial and boundary conditions.
Contribution: Monotone schemes for anisotropic problems.

Anisotropic diffusion

Given a diffusion tensor field $D : \Omega \subseteq \mathbb{R}^d \to S_d^{++}$, takes the form

$$\partial_t u = \operatorname{div}(D \nabla u),$$

with suitable initial and boundary conditions.
Contribution: Monotone schemes for anisotropic problems.

Applications:

- Image processing, with J. Fehrenbach. $(D = D(u))$

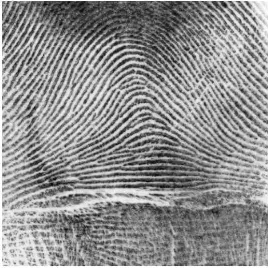

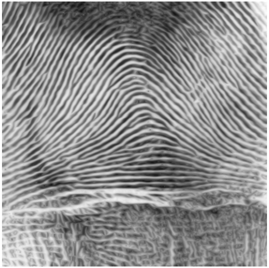

Anisotropic diffusion

Given a diffusion tensor field $D : \Omega \subseteq \mathbb{R}^d \to S_d^{++}$, takes the form

$$\partial_t u = \operatorname{div}(D \nabla u),$$

with suitable initial and boundary conditions.

Contribution: Monotone schemes for anisotropic problems.

Applications:

- Image processing, with J. Fehrenbach. ($D = D(u)$)

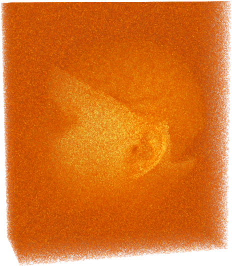

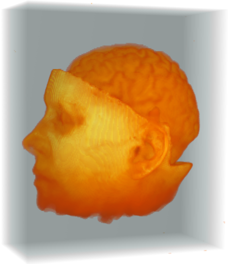

Anisotropic diffusion

Given a diffusion tensor field $D : \Omega \subseteq \mathbb{R}^d \to S_d^{++}$, takes the form

$$\partial_t u = \mathrm{div}(D \nabla u),$$

with suitable initial and boundary conditions.
Contribution: Monotone schemes for anisotropic problems.

Applications:

- Image processing, with J. Fehrenbach. ($D = D(u)$)

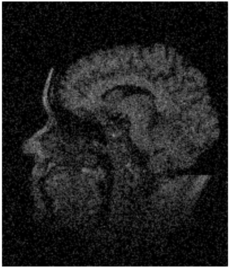

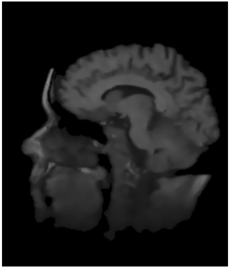

Anisotropic diffusion

Given a diffusion tensor field $D : \Omega \subseteq \mathbb{R}^d \to S_d^{++}$, takes the form

$$\partial_t u = \mathrm{Tr}(D\nabla^2 u),$$

with suitable initial and boundary conditions.
Contribution: Monotone schemes for anisotropic problems.

Applications:

- Image processing, with J. Fehrenbach. $(D = D(u))$
- Non-divergence form anisotropic diffusion.
- Monge-Ampere operator, with Benamou, Collino.
- Perspectives: HJB PDEs of stochastic models, F. Bonnans.

Introduction: anisotropy and cartesian grids

Problems addressed

Finslerian eikonal equations, and the Stern-Brocot tree
- Semi-Lagrangian schemes
- Adaptive stencil refinement
- Application to image segmentation

Riemannian eikonal equations, and Voronoi's reduction
- Monotone and causal schemes
- Grid-adapted tensor decomposition

Global optimization of curvature dependent energies
- The Reeds-Shepp models
- Euler-Mumford elastica curves, and others

Conclusion

Introduction: anisotropy and cartesian grids

Problems addressed

Finslerian eikonal equations, and the Stern-Brocot tree
- Semi-Lagrangian schemes
- Adaptive stencil refinement
- Application to image segmentation

Riemannian eikonal equations, and Voronoi's reduction
- Monotone and causal schemes
- Grid-adapted tensor decomposition

Global optimization of curvature dependent energies
- The Reeds-Shepp models
- Euler-Mumford elastica curves, and others

Conclusion

Context: Domain Ω, local metric $\mathcal{F} : T\Omega \to \mathbb{R}^+$ defining

$$d_{\mathcal{F}}(x, y) := \inf_{\gamma} \int_0^1 \mathcal{F}_{\gamma(t)}(\gamma'(t))\, \mathrm{d}t \quad \text{s.t.} \begin{cases} \gamma \in \mathrm{Lip}_{\mathrm{loc}}([0,1], \overline{\Omega}) \\ \gamma(0) = x, \gamma(1) = y. \end{cases}$$

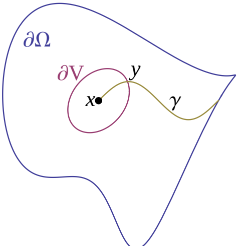

Context: Domain Ω, local metric $\mathcal{F} : T\Omega \to \mathbb{R}^+$ defining

$$d_{\mathcal{F}}(x, y) := \inf_{\gamma} \int_0^1 \mathcal{F}_{\gamma(t)}(\gamma'(t))\, \mathrm{d}t \quad \text{s.t.} \begin{cases} \gamma \in \mathrm{Lip}_{\mathrm{loc}}([0,1], \overline{\Omega}) \\ \gamma(0) = x, \gamma(1) = y. \end{cases}$$

Objective: Compute numerically the exit time to the boundary

$$u(x) = \min_{y \in \partial\Omega} d_{\mathcal{F}}(x, y).$$

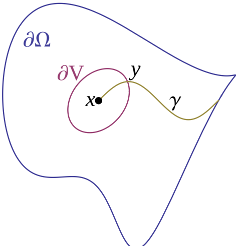

Context: Domain Ω, local metric $\mathcal{F} : T\Omega \to \mathbb{R}^+$ defining

$$d_{\mathcal{F}}(x,y) := \inf_{\gamma} \int_0^1 \mathcal{F}_{\gamma(t)}(\gamma'(t))\,\mathrm{d}t \quad \text{s.t.} \begin{cases} \gamma \in \mathrm{Lip}_{\mathrm{loc}}([0,1], \overline{\Omega}) \\ \gamma(0) = x, \gamma(1) = y. \end{cases}$$

Objective: Compute numerically the exit time to the boundary

$$u(x) = \min_{y \in \partial\Omega} d_{\mathcal{F}}(x,y).$$

Bellman's optimality principle

For any neighborhood V of x contained in Ω.

$$u(x) = \min_{y \in \partial V} \Big(d_{\mathcal{F}}(x,y) + u(y) \Big).$$

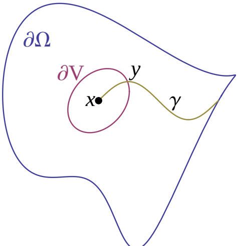

Context: Finite sets X, ∂X approximating $\Omega, \partial\Omega$. Polyhedral neighborhood $V(x)$, of each $x \in X$, with vertices in $X \cup \partial X$.

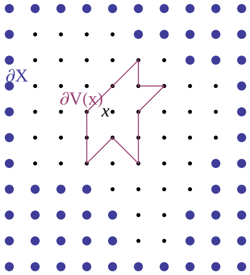

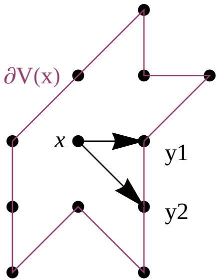

Context: Finite sets X, ∂X approximating $\Omega, \partial\Omega$. Polyhedral neighborhood $V(x)$, of each $x \in X$, with vertices in $X \cup \partial X$.

Semi-Lagrangian discretization

Find $U : X \cup \partial X \to \mathbb{R}$, vanishing on ∂X, and such that $\forall x \in X$

$$U(x) = \min_{y \in \partial V(x)} \Big(\mathcal{F}_x(y - x) + \mathrm{I}_{V(x)}\, U(y) \Big).$$

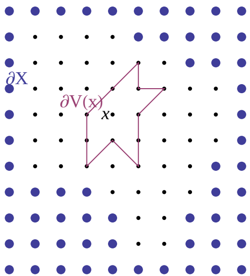

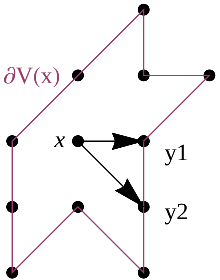

Discretization yields a coupled system of non-linear equations.

$$\forall x \in X, U(x) = \Lambda U(x), \qquad \forall x \in \partial X, U(x) = 0. \qquad (1)$$

Discretization yields a coupled system of non-linear equations.

$$\forall x \in X, U(x) = \Lambda U(x), \qquad \forall x \in \partial X, U(x) = 0. \tag{1}$$

Analogous problem: computing shortest paths on graphs

Neighbors $S(x)$ of $x \in X$, edge lengths $w(x, y)$, operator

$$\Lambda U(x) = \min_{y \in S(x)} \Big(w(x, y) + U(y) \Big).$$

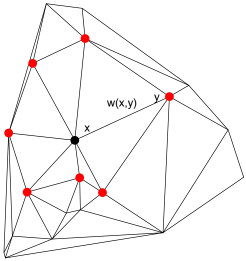

Discretization yields a coupled system of non-linear equations.

$$\forall x \in X, U(x) = \Lambda U(x), \qquad \forall x \in \partial X, U(x) = 0. \tag{1}$$

Analogous problem: computing shortest paths on graphs

Neighbors $S(x)$ of $x \in X$, edge lengths $w(x,y)$, operator

$$\Lambda U(x) = \min_{y \in S(x)} \Big(w(x,y) + U(y) \Big).$$

System (1) is solvable in a single pass by Dijkstra's algorithm iff

$$w(x,y) \geq 0 \text{ for all } x \in X,\ y \in S(x).$$

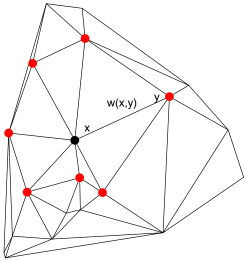

Discretization yields a coupled system of non-linear equations.

$$\forall x \in X, U(x) = \Lambda U(x), \qquad \forall x \in \partial X, U(x) = 0. \qquad (1)$$

Analogous problem: computing shortest paths on graphs

Neighbors $S(x)$ of $x \in X$, edge lengths $w(x,y)$, operator

$$\Lambda U(x) = \min_{y \in S(x)} \Big(w(x,y) + U(y) \Big).$$

System (1) is solvable in a single pass by Dijkstra's algorithm iff

$$w(x,y) \geq 0 \text{ for all } x \in X,\ y \in S(x).$$

Acuteness implies causality (Sethian, Kimmel, Vladimirsky, 96)

System (1) is solvable by the fast marching method, in a single pass, iff

$$(u,v) \text{ make an } \mathcal{F}_x\text{-acute angle,}$$

whenever $x+u$, $x+v$ lie in a common facet of $V(x)$.

What is an acute angle ? (Sethian,Kimmel,Vladimirsky,96)

Vectors $u, v \in \mathbb{E} = \mathbb{R}^d$, make an F-acute angle, where $F : \mathbb{E} \to \mathbb{R}_+$ an asymmetric norm, iff

- (Euclidean case) Assuming $F(x) = m\|x\|$, where $m > 0$,

$$\langle u, v \rangle \geq 0.$$

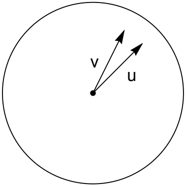

What is an acute angle ? (Sethian,Kimmel,Vladimirsky,96)

Vectors $u, v \in \mathbb{E} = \mathbb{R}^d$, make an F-acute angle, where $F : \mathbb{E} \to \mathbb{R}_+$ an asymmetric norm, iff

- (Euclidean case) Assuming $F(x) = m\|x\|$, where $m > 0$,

$$\langle u, v\rangle \geq 0.$$

- (Riemannian case) Assuming $F(x) = \|x\|_M$, where $M \succ 0$,

$$\langle u, Mv\rangle \geq 0.$$

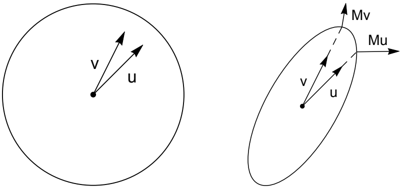

Introduction

Panorama

Finslerian eikonal

Semi-Lagrangian schemes

Adaptive stencil refinement

Image segmentation

Riemannian eikonal

Monotony and causality

Grid-adapted tensor decomposition

Curvature penalization

Reeds-Shepp

Other models

Conclusion

What is an acute angle ? (Sethian,Kimmel,Vladimirsky,96)

Vectors $u, v \in \mathbb{E} = \mathbb{R}^d$, make an F-acute angle, where $F : \mathbb{E} \to \mathbb{R}_+$ an asymmetric norm, iff

- (Euclidean case) Assuming $F(x) = m\|x\|$, where $m > 0$,

$$\langle u, v\rangle \geq 0.$$

- (Riemannian case) Assuming $F(x) = \|x\|_M$, where $M \succ 0$,

$$\langle u, Mv\rangle \geq 0.$$

- (Differentiable case) $\langle \nabla F(u), v\rangle \geq 0$, and $\langle \nabla F(v), u\rangle \geq 0$.

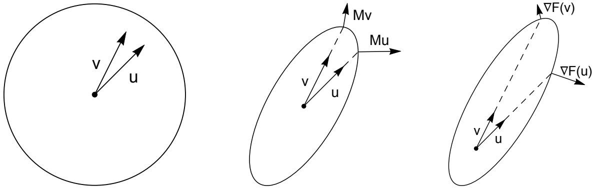

What is an acute angle ? (Sethian,Kimmel,Vladimirsky,96)

Vectors $u, v \in \mathbb{E} = \mathbb{R}^d$, make an F-acute angle, where $F : \mathbb{E} \to \mathbb{R}_+$ an asymmetric norm, iff

- (Euclidean case) Assuming $F(x) = m\|x\|$, where $m > 0$,
$$\langle u, v\rangle \geq 0.$$
- (Riemannian case) Assuming $F(x) = \|x\|_M$, where $M \succ 0$,
$$\langle u, Mv\rangle \geq 0.$$
- (Differentiable case) $\langle \nabla F(u), v\rangle \geq 0$, and $\langle \nabla F(v), u\rangle \geq 0$.

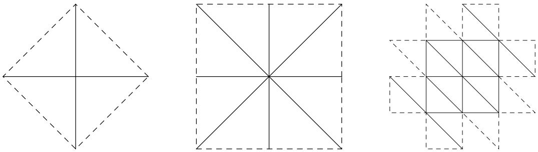

Figure: Stencil constructions proposed for isotropic (left), or midly anisotropic metrics, due to Sethian, Kimmel, Alton, ...

Introduction: anisotropy and cartesian grids

Problems addressed

Finslerian eikonal equations, and the Stern-Brocot tree

- Semi-Lagrangian schemes
- Adaptive stencil refinement
- Application to image segmentation

Riemannian eikonal equations, and Voronoi's reduction

- Monotone and causal schemes
- Grid-adapted tensor decomposition

Global optimization of curvature dependent energies

- The Reeds-Shepp models
- Euler-Mumford elastica curves, and others

Conclusion

Fast-Marching using Adaptive Stencil Refinement

- Iterative refinement of the stencil until the acuteness property is met. (FM-ASR scheme, on 2D cartesian grids)

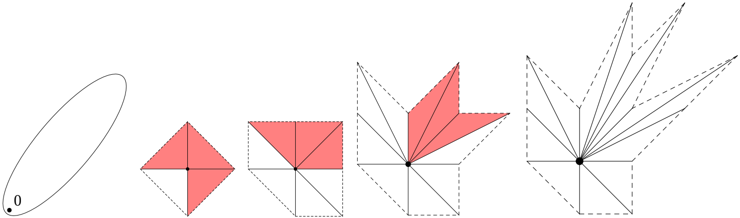

Fast-Marching using Adaptive Stencil Refinement

- Iterative refinement of the stencil until the acuteness property is met. (FM-ASR scheme, on 2D cartesian grids)

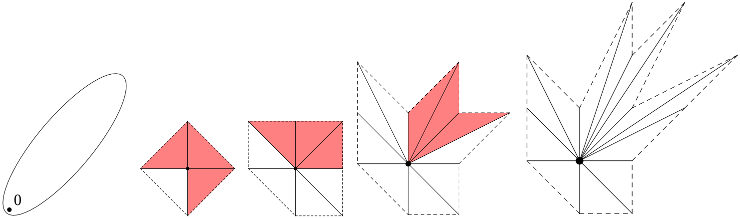

- The splitting procedure is exploits the grid additivity.

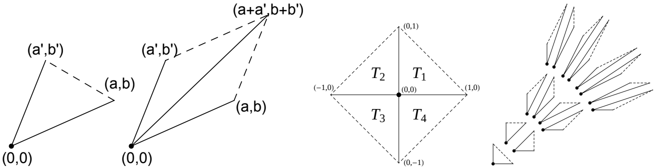

Fast-Marching using Adaptive Stencil Refinement

- Iterative refinement of the stencil until the acuteness property is met. (FM-ASR scheme, on 2D cartesian grids)

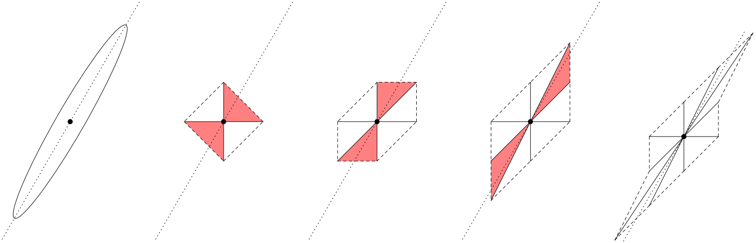

- The splitting procedure is exploits the grid additivity.

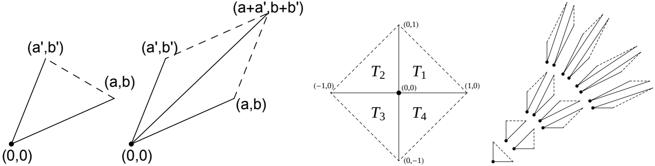

The Stern Brocot tree

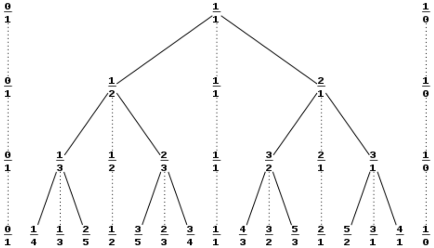

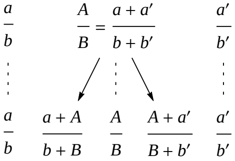

Obtain the $(n+1)$-th line by inserting $\frac{a+a'}{b+b'}$ between consecutive elements $\frac{a}{b}$ and $\frac{a'}{b'}$ of the n-th line.

- Each positive rational number appears exactly once in the tree, in its irreducible form.
- Well studied arithmetic object, used for rational approximation.

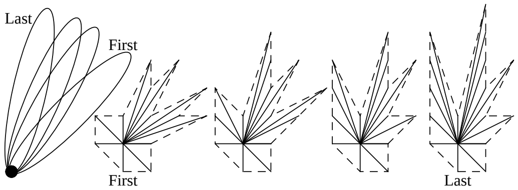

Context: F asymmetric norm on $\mathbb{R}^2$, $\mathcal{T}(F)$ the FM-ASR stencil,

$$\mu(F) := \max_{|u|=|v|=1} \frac{F(u)}{F(v)}.$$

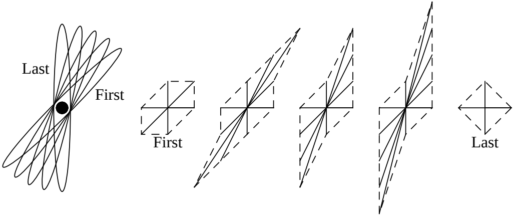

Context: F asymmetric norm on $\mathbb{R}^2$, $\mathcal{T}(F)$ the FM-ASR stencil,

$$\mu(F) := \max_{|u|=|v|=1} \frac{F(u)}{F(v)}.$$

Theorem (Worst and average stencil size)

For any asymmetric norm F on $\mathbb{R}^2$, denoting by R_θ the rotation of angle θ, one has $\#(\mathcal{T}(F)) \leq C\mu \ln \mu$, and

$$\int_0^{2\pi} \#(\mathcal{T}(F \circ R_\theta))\, \mathrm{d}\theta \leq C \ln^3 \mu$$

where $\mu := \max\{2, \mu(F)\}$, and C is an absolute constant.

Introduction: anisotropy and cartesian grids

Problems addressed

Finslerian eikonal equations, and the Stern-Brocot tree

- Semi-Lagrangian schemes
- Adaptive stencil refinement
- Application to image segmentation

Riemannian eikonal equations, and Voronoi's reduction

- Monotone and causal schemes
- Grid-adapted tensor decomposition

Global optimization of curvature dependent energies

- The Reeds-Shepp models
- Euler-Mumford elastica curves, and others

Conclusion

Region segmentation using Rander geodesics

Define for any region $\Omega \subseteq \mathbb{R}^2$ the energy

$$\mathcal{E}(\Omega) := \int_\Omega f(x)\mathrm{d}x + \int_{\partial\Omega} g(x)\mathrm{d}x.$$

- Joint work with Laurent Cohen, Da Chen.

Region segmentation using Rander geodesics

Define for any region $\Omega \subseteq \mathbb{R}^2$ the energy

$$\mathcal{E}(\Omega) := \int_\Omega f(x)\mathrm{d}x + \int_{\partial\Omega} g(x)\mathrm{d}x.$$

Assuming $f = \operatorname{div} w$, this rewrites as

$$\mathcal{E}(\Omega) = \int_{\partial\Omega} (\langle w(x), n(x)\rangle + g(x))\mathrm{d}x = \int_0^1 \mathcal{F}_{\gamma(t)}(\gamma'(t))\,\mathrm{d}t,$$

where $\gamma : [0,1] \to \mathbb{R}^2$ parametrizes $\partial\Omega$ counter clockwise, and

$$\mathcal{F}_x(v) := g(x)\|v\| + \langle w(x)^\perp, v\rangle.$$

- Joint work with Laurent Cohen, Da Chen.

Region segmentation using Rander geodesics

Define for any region $\Omega \subseteq \mathbb{R}^2$ the energy

$$\mathcal{E}(\Omega) := \int_\Omega f(x)\mathrm{d}x + \int_{\partial\Omega} g(x)\mathrm{d}x.$$

Assuming $f = \operatorname{div} w$, this rewrites as

$$\mathcal{E}(\Omega) = \int_{\partial\Omega} (\langle w(x), n(x)\rangle + g(x))\mathrm{d}x = \int_0^1 \mathcal{F}_{\gamma(t)}(\gamma'(t))\,\mathrm{d}t,$$

where $\gamma : [0,1] \to \mathbb{R}^2$ parametrizes $\partial\Omega$ counter clockwise, and

$$\mathcal{F}_x(v) := g(x)\|v\| + \langle w(x)^\perp, v\rangle.$$

- A *Rander* metric, provided $|w(x)| < g(x)$ for all x.
- Joint work with Laurent Cohen, Da Chen.

Region segmentation using Rander geodesics

Define for any region $\Omega \subseteq \mathbb{R}^2$ the energy

$$\mathcal{E}(\Omega) := \int_\Omega f(x)\mathrm{d}x + \int_{\partial\Omega} g(x)\mathrm{d}x.$$

Assuming $f = \operatorname{div} w$, this rewrites as

$$\mathcal{E}(\Omega) = \int_{\partial\Omega} (\langle w(x), n(x)\rangle + g(x))\mathrm{d}x = \int_0^1 \mathcal{F}_{\gamma(t)}(\gamma'(t))\,\mathrm{d}t,$$

where $\gamma : [0,1] \to \mathbb{R}^2$ parametrizes $\partial\Omega$ counter clockwise, and

$$\mathcal{F}_x(v) := g(x)\|v\| + \langle w(x)^\perp, v\rangle.$$

- A *Rander* metric, provided $|w(x)| < g(x)$ for all x.
- Ω is (locally) optimal iff $\partial\Omega$ is a geodesic.
- Joint work with Laurent Cohen, Da Chen.

- Compute the field w by solving an elliptic equation:

$$\Delta p = f \qquad \Rightarrow \qquad \operatorname{div}(w) = f \text{ where } w = \nabla p.$$

- Extract the minimizing Rander geodesics between some known boundary points.

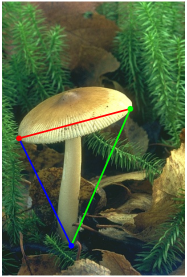

- Compute the field w by solving an elliptic equation:

$$\Delta p = f \qquad\qquad \Rightarrow \quad \mathrm{div}(w) = f \text{ where } w = \nabla p.$$

- Extract the minimizing Rander geodesics between some known boundary points.
- The method is actually iterative, due to constraint $|w| < g$, and so as to accept approximate boundary points.

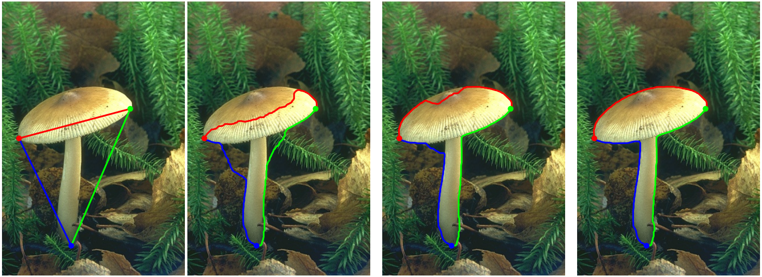

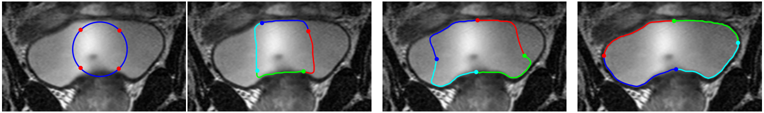

- Compute the field w by solving an elliptic equation:

$$\Delta p = f \text{ on } U \supseteq \partial\Omega \quad \Rightarrow \quad \mathrm{div}(w) = f \text{ where } w = \nabla p.$$

- Extract the minimizing Rander geodesics between some known boundary points.
- The method is actually iterative, due to constraint $|w| < g$, and so as to accept approximate boundary points.

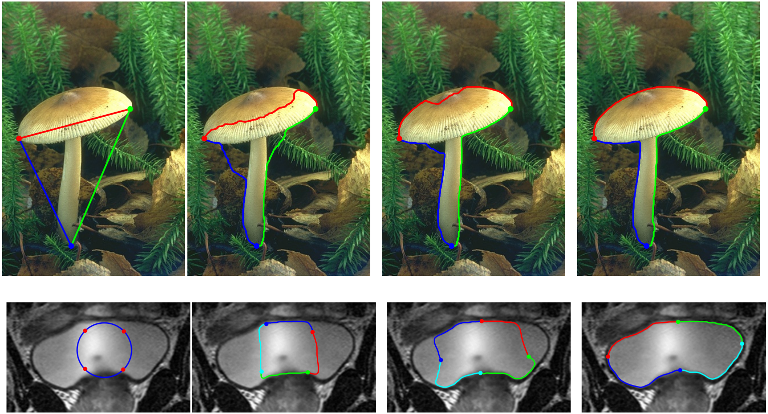

Introduction: anisotropy and cartesian grids

Problems addressed

Finslerian eikonal equations, and the Stern-Brocot tree
- Semi-Lagrangian schemes
- Adaptive stencil refinement
- Application to image segmentation

Riemannian eikonal equations, and Voronoi's reduction
- Monotone and causal schemes
- Grid-adapted tensor decomposition

Global optimization of curvature dependent energies
- The Reeds-Shepp models
- Euler-Mumford elastica curves, and others

Conclusion

Introduction: anisotropy and cartesian grids

Problems addressed

Finslerian eikonal equations, and the Stern-Brocot tree
- Semi-Lagrangian schemes
- Adaptive stencil refinement
- Application to image segmentation

Riemannian eikonal equations, and Voronoi's reduction
- Monotone and causal schemes
- Grid-adapted tensor decomposition

Global optimization of curvature dependent energies
- The Reeds-Shepp models
- Euler-Mumford elastica curves, and others

Conclusion

A generalized finite differences scheme takes the form:

$$FU(x) := F(x, U(x), (U(x) - U(y))_{y \in X}),$$

where X is a finite set, and $U : X \to \mathbb{E}$. Desirable properties:

Scheme for isotropic eikonal eqns (Rouy 92, Sethian 96)

At first order, denoting $(e_i)_{1 \leq i \leq d}$ the canonical basis of $\mathbb{R}^d$,

$$\|\nabla u(x)\|^2 \approx h^{-2} \sum_{1 \leq i \leq d} \max\{0,\ u(x) - u(x - he_i),\ u(x) - u(x + he_i)\}^2$$

A generalized finite differences scheme takes the form:

$$FU(x) := F(x, U(x), (U(x) - U(y))_{y \in X}),$$

where X is a finite set, and $U : X \to \mathbb{E}$. Desirable properties:

Monotony

F is non-decreasing in its second and (each) third variable.

- Yields comparison princples, used for convergence analysis.

Scheme for isotropic eikonal eqns (Rouy 92, Sethian 96)

At first order, denoting $(e_i)_{1 \leq i \leq d}$ the canonical basis of $\mathbb{R}^d$,

$$\|\nabla u(x)\|^2 \approx h^{-2} \sum_{1 \leq i \leq d} \max\{0,\ u(x) - u(x - he_i),\ u(x) - u(x + he_i)\}^2$$

A generalized finite differences scheme takes the form:

$$FU(x) := F(x, U(x), (U(x) - U(y))_{y \in X}),$$

where X is a finite set, and $U : X \to \mathbb{E}$. Desirable properties:

Monotony

F is non-decreasing in its second and (each) third variable.

- Yields comparison princples, used for convergence analysis.

Causality

F only depends on the positive part of (each) third variable.

- Enables solving $FU \equiv 0$ in a single pass, using the fast-marching method ($\sim$ Dijkstra's algorithm).

Scheme for isotropic eikonal eqns (Rouy 92, Sethian 96)

At first order, denoting $(e_i)_{1 \leq i \leq d}$ the canonical basis of $\mathbb{R}^d$,

$$\|\nabla u(x)\|^2 \approx h^{-2} \sum_{1 \leq i \leq d} \max\{0,\ u(x) - u(x - he_i),\ u(x) - u(x + he_i)\}^2$$

Introduction: anisotropy and cartesian grids

Problems addressed

Finslerian eikonal equations, and the Stern-Brocot tree
- Semi-Lagrangian schemes
- Adaptive stencil refinement
- Application to image segmentation

Riemannian eikonal equations, and Voronoi's reduction
- Monotone and causal schemes
- Grid-adapted tensor decomposition

Global optimization of curvature dependent energies
- The Reeds-Shepp models
- Euler-Mumford elastica curves, and others

Conclusion

W generalize the isotropic scheme using tensor decompositions

$$D = \sum_{1 \leq i \leq I} \lambda_i e_i e_i^{\mathrm{T}},$$

with non-negative weights $\lambda_i \geq 0$, and integer offsets $e_i \in \mathbb{Z}^d$.

- We select an admissible decomposition maximizing

$$\sum_{1 \leq i \leq I} \lambda_i.$$

  Optimal solution has $I = d(d+1)/2$.
- The resulting linear program is known as Voronoi's first reduction (dual), and widely studied.
- Symmetries enable extremely fast resolution (one per discretization point).

Fast Marching using Voronoi's First Reduction

At first order, assuming a decomposition $D = \sum_{i=1}^{I} \lambda_i e_i e_i^{\mathrm{T}}$,

$$\|\nabla u(x)\|_D^2 \approx \frac{1}{h^2} \sum_{1 \leq i \leq I} \lambda_i \max\{0, u(x) - u(x - he_i), u(x) - u(x + he_i)\}^2$$

Fast Marching using Voronoi's First Reduction

At first order, assuming a decomposition $D = \sum_{i=1}^{I} \lambda_i e_i e_i^{\mathrm{T}}$,

$$\|\nabla u(x)\|_D^2 \approx \frac{1}{h^2} \sum_{1 \leq i \leq I} \lambda_i \max\{0, u(x)-u(x-he_i), u(x)-u(x+he_i)\}^2$$

- Number of terms: $I = d(d+1)/2$.

Fast Marching using Voronoi's First Reduction

At first order, assuming a decomposition $D = \sum_{i=1}^{I} \lambda_i e_i e_i^{\mathrm{T}}$,

$$\|\nabla u(x)\|_D^2 \approx \frac{1}{h^2} \sum_{1 \leq i \leq I} \lambda_i \max\{0, u(x) - u(x - he_i), u(x) - u(x + he_i)\}^2$$

- Number of terms: $I = d(d+1)/2$.
- Reduces to the original scheme if $D = \lambda\,\mathrm{Id}$.

Fast Marching using Voronoi's First Reduction

At first order, assuming a decomposition $D = \sum_{i=1}^{I} \lambda_i e_i e_i^{\mathrm{T}}$,

$$\|\nabla u(x)\|_D^2 \approx \frac{1}{h^2} \sum_{1 \leq i \leq I} \lambda_i \max\{0, u(x)-u(x-he_i), u(x)-u(x+he_i)\}^2$$

- Number of terms: $I = d(d+1)/2$.
- Reduces to the original scheme if $D = \lambda \,\mathrm{Id}$.
- Implemented in dimensions 2 to 5.

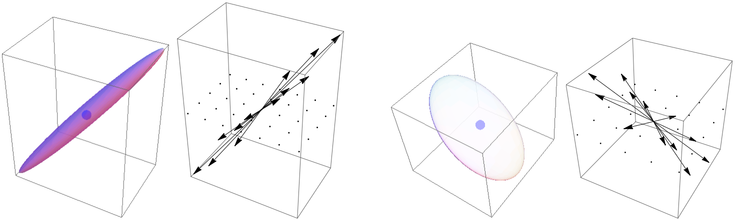

Figure: Unit ball defined by D^{-1}, and offsets e_i appearing in the decomposition of D associated with Voronoi's first reduction.

Fast Marching using Voronoi's First Reduction

At first order, assuming a decomposition $D = \sum_{i=1}^{I} \lambda_i e_i e_i^{\mathrm{T}}$,

$$\|\nabla u(x)\|_D^2 \approx \frac{1}{h^2} \sum_{1 \leq i \leq I} \lambda_i \max\{0, u(x) - u(x - he_i), u(x) - u(x + he_i)\}^2$$

- Number of terms: $I = d(d+1)/2$.
- Reduces to the original scheme if $D = \lambda\, \mathrm{Id}$.
- Implemented in dimensions 2 to 5.

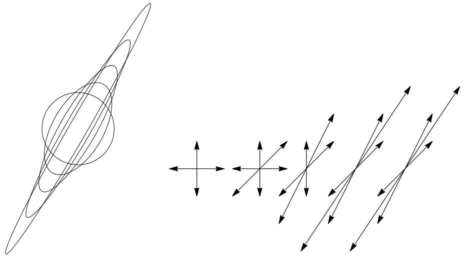

Figure: Unit ball defined by D^{-1}, and offsets e_i appearing in the decomposition of D associated with Voronoi's first reduction.

Fast Marching using Voronoi's First Reduction

At first order, assuming a decomposition $D = \sum_{i=1}^{I} \lambda_i e_i e_i^{\mathrm{T}}$,

$$\|\nabla u(x)\|_D^2 \approx \frac{1}{h^2} \sum_{1 \leq i \leq I} \lambda_i \max\{0, u(x)-u(x-he_i), u(x)-u(x+he_i)\}^2$$

- Number of terms: $I = d(d+1)/2$.
- Reduces to the original scheme if $D = \lambda\, \mathrm{Id}$.
- Implemented in dimensions 2 to 5.

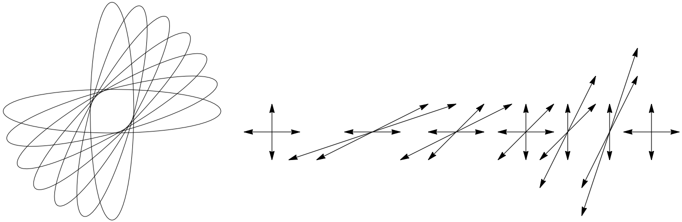

Figure: Unit ball defined by D^{-1}, and offsets e_i appearing in the decomposition of D associated with Voronoi's first reduction.

Fast Marching using Voronoi's First Reduction

At first order, assuming a decomposition $D = \sum_{i=1}^{I} \lambda_i e_i e_i^{\mathrm{T}}$,

$$\|\nabla u(x)\|_D^2 \approx \frac{1}{h^2} \sum_{1 \leq i \leq I} \lambda_i \max\{0, u(x) - u(x - he_i), u(x) - u(x + he_i)\}^2$$

- Number of terms: $I = d(d+1)/2$.
- Reduces to the original scheme if $D = \lambda \, \mathrm{Id}$.
- Implemented in dimensions 2 to 5.

Theorem

For each $\mu \geq 1$ and $\theta \in [0, 2\pi]$, denote $r_\mu(\theta) := \max_{1 \leq i \leq I} \|e_i\|$ where $(\lambda_i, e_i)_{1 \leq i \leq I}$ comes from the decomposition of

$$\mu^{-1} e(\theta) \otimes e(\theta) + \mu e(\theta)^\perp \otimes e(\theta)^\perp.$$

Then, as $\mu \to \infty$

$$\|r_\mu\|_{L^p([0,2\pi])} \asymp \begin{cases} \mu^{1-1/p} & \text{if } 2 < p \leq \infty \\ \sqrt{\mu \ln \mu} & \text{if } p = 2 \\ \sqrt{\mu} & \text{if } 1 \leq p < 2. \end{cases}$$

Introduction: anisotropy and cartesian grids

Problems addressed

Finslerian eikonal equations, and the Stern-Brocot tree
- Semi-Lagrangian schemes
- Adaptive stencil refinement
- Application to image segmentation

Riemannian eikonal equations, and Voronoi's reduction
- Monotone and causal schemes
- Grid-adapted tensor decomposition

Global optimization of curvature dependent energies
- The Reeds-Shepp models
- Euler-Mumford elastica curves, and others

Conclusion

Introduction: anisotropy and cartesian grids

Problems addressed

Finslerian eikonal equations, and the Stern-Brocot tree
- Semi-Lagrangian schemes
- Adaptive stencil refinement
- Application to image segmentation

Riemannian eikonal equations, and Voronoi's reduction
- Monotone and causal schemes
- Grid-adapted tensor decomposition

Global optimization of curvature dependent energies
- The Reeds-Shepp models
- Euler-Mumford elastica curves, and others

Conclusion

The Reeds-Shepp model

Configuration space $\mathbb{M}_2 := \mathbb{R}^2 \times \mathbb{S}^1$, positions and orientations.

$$\|(\dot{x}, \dot{n})\|^2_{\mathcal{M}(x,n)} := c(x,n)^2 \Big(\langle n, \dot{x}\rangle^2 + \varepsilon^{-2} \langle n^\perp, \dot{x}\rangle^2 + \|\dot{n}\|^2 \Big).$$

- Theoretically, $\varepsilon \to 0$ and the model is sub-Riemannian.
- Numerically, good results obtained with $\varepsilon = 0.1$.

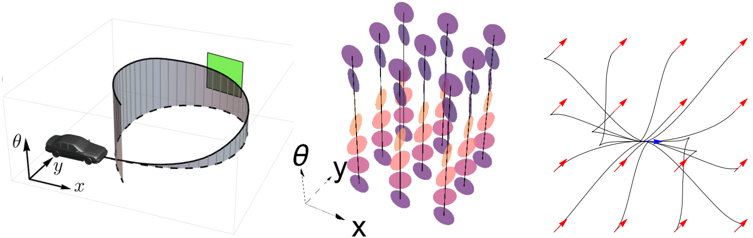

- Parametrization $n = (\cos\theta, \sin\theta)$, $\theta \in [0, 2\pi]$, of $\mathbb{S}^1$.

Application to tubular structure segmentation

- Segmenting the retinal vascular tree using Reeds-Shepp model, with data driven $c(x, n)$. With R. Duits et al.

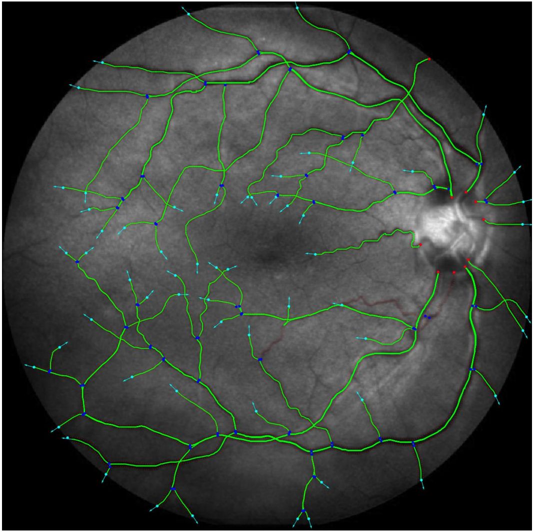

Application to tubular structure segmentation

- Segmenting the retinal vascular tree using Reeds-Shepp model, with data driven $c(x, n)$. With R. Duits et al.

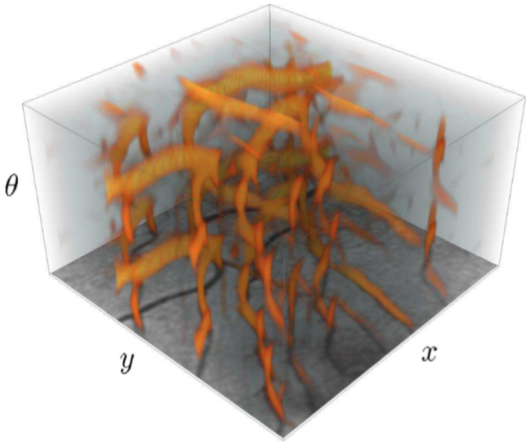

Figure: Density plot of the cost function $c(x, y, \theta)$.
Related: (radius lift) Li and Yezzi 07, (θ lift) Péchaud et al 09.

Higher dimensional Reeds-Shepp model

The model extends to $\mathbb{R}^3 \times \mathbb{S}^2$,

$$\|(\dot{x}, \dot{n})\|^2_{\mathcal{M}(x,n)} := c(x, n)^2 \Big(\langle n, \dot{x} \rangle^2 + \varepsilon^{-2} \|P_n(\dot{x})\|^2 + \|\dot{n}\|^2 \Big).$$

where $P_n := \mathrm{Id} - n \otimes n$ is the orthogonal projection onto $(\mathbb{R}n)^\perp$.

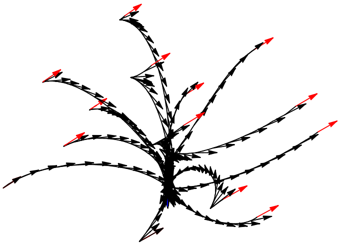

Figure: Left: $P_n(\dot{x}) = 0$.

Higher dimensional Reeds-Shepp model(s)

The model extends to $\mathbb{R}^3 \times \mathbb{S}^2$, and has an unexpected variant.

$$\|(\dot{x}, \dot{n})\|^2_{\mathcal{M}(x,n)} := c(x,n)^2 \Big(\langle n, \dot{x} \rangle^2 + \varepsilon^{-2} \|P_n(\dot{x})\|^2 + \|\dot{n}\|^2 \Big).$$

$$\|(\dot{x}, \dot{n})\|^2_{\widetilde{\mathcal{M}}(x,n)} := c(x,n)^2 \Big(\varepsilon^{-2} \langle n, \dot{x} \rangle^2 + \|P_n(\dot{x})\|^2 + \|\dot{n}\|^2 \Big).$$

where $P_n := \mathrm{Id} - n \otimes n$ is the orthogonal projection onto $(\mathbb{R}n)^\perp$.

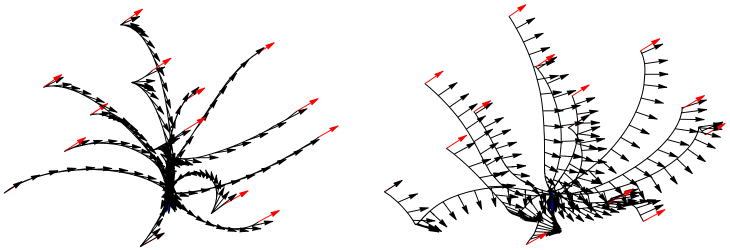

Figure: Left: $P_n(\dot{x}) = 0$. Right: $\langle n, \dot{x} \rangle = 0$.

Determination of the connectivity of white matter fibers, on dMRI data, with R. Duits et al

- Difficulty: some fiber bundles cross each other.
- Our solution: minimal paths w.r.t. the Reeds-Shepp model, imposing directional consistency, with suitable $c(x, n)$.

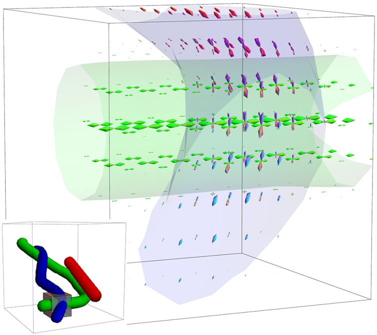

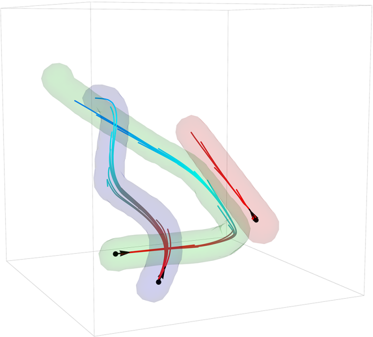

Determination of the connectivity of white matter fibers, on dMRI data, with R. Duits et al

- Difficulty: some fiber bundles cross each other.
- Our solution: minimal paths w.r.t. the Reeds-Shepp model, imposing directional consistency, with suitable $c(x, n)$.

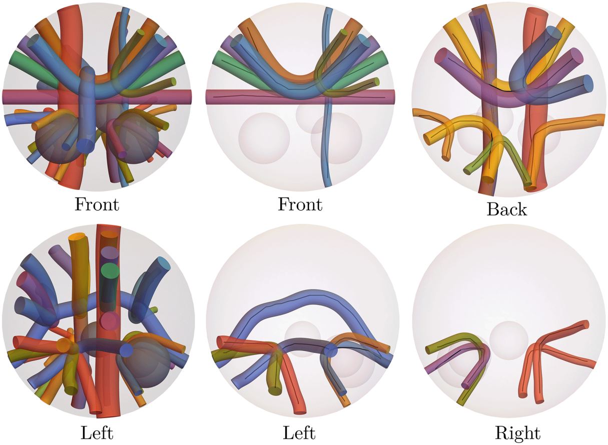

Introduction: anisotropy and cartesian grids

Problems addressed

Finslerian eikonal equations, and the Stern-Brocot tree
- Semi-Lagrangian schemes
- Adaptive stencil refinement
- Application to image segmentation

Riemannian eikonal equations, and Voronoi's reduction
- Monotone and causal schemes
- Grid-adapted tensor decomposition

Global optimization of curvature dependent energies
- The Reeds-Shepp models
- Euler-Mumford elastica curves, and others

Conclusion

Curvature penalized planar paths

The Reeds-Shepp model penalizes path curvature, but it:

- Allows for cusps (shift into reverse gear).
- Has specific cost dependency $\sqrt{1+\kappa^2}$, w.r.t. curvature κ.

Curvature penalized planar paths

The Reeds-Shepp model penalizes path curvature, but it:

- Allows for cusps (shift into reverse gear).
- Has specific cost dependency $\sqrt{1+\kappa^2}$, w.r.t. curvature κ.

Generalizing the previous approach, we compute paths globally minimizing various curvature dependent energies.

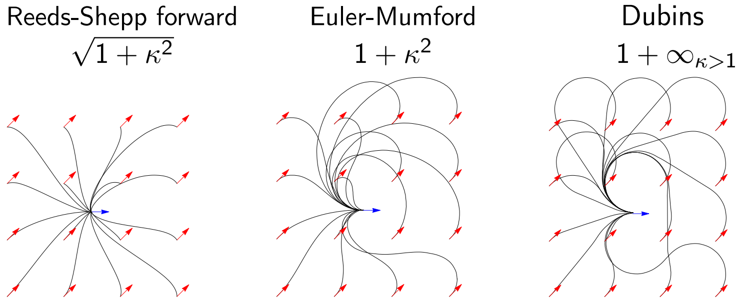

Figure: Minimal paths, in free space.

Curvature penalized planar paths

The Reeds-Shepp model penalizes path curvature, but it:

- Allows for cusps (shift into reverse gear).
- Has specific cost dependency $\sqrt{1+\kappa^2}$, w.r.t. curvature κ.

Generalizing the previous approach, we compute paths globally minimizing various curvature dependent energies.

Reeds-Shepp forward	Euler-Mumford	Dubins
$\sqrt{1+\kappa^2}$	$1+\kappa^2$	$1+\infty_{\kappa>1}$

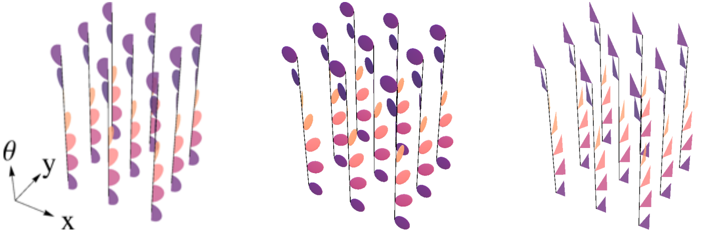

Figure: Control sets of the different models

Curvature penalized planar paths

The Reeds-Shepp model penalizes path curvature, but it:

- Allows for cusps (shift into reverse gear).
- Has specific cost dependency $\sqrt{1+\kappa^2}$, w.r.t. curvature κ.

Generalizing the previous approach, we compute paths globally minimizing various curvature dependent energies.

Reeds-Shepp forward $\sqrt{1+\kappa^2}$ | Euler-Mumford $1+\kappa^2$ | Dubins $1+\infty_{\kappa>1}$

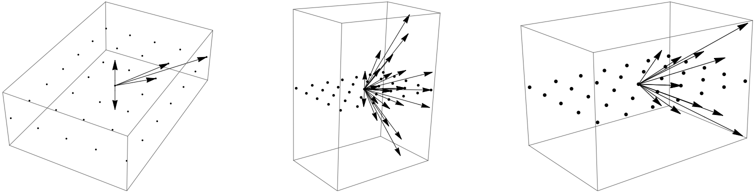

Figure: Stencils used for the eikonal PDE discretization.

Curvature penalized planar paths

The Reeds-Shepp model penalizes path curvature, but it:

- Allows for cusps (shift into reverse gear).
- Has specific cost dependency $\sqrt{1+\kappa^2}$, w.r.t. curvature κ.

Generalizing the previous approach, we compute paths globally minimizing various curvature dependent energies.

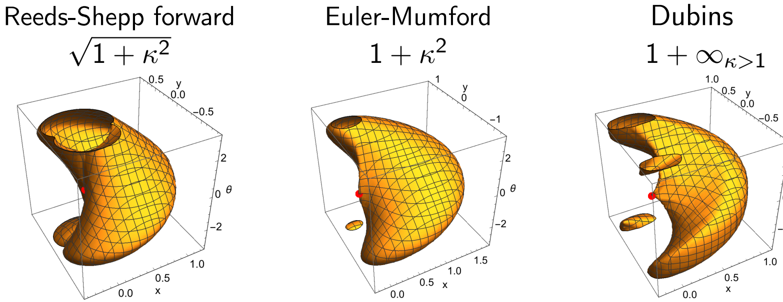

Figure: Level set of the distance function.

Curvature penalized planar paths

The Reeds-Shepp model penalizes path curvature, but it:

- Allows for cusps (shift into reverse gear).
- Has specific cost dependency $\sqrt{1+\kappa^2}$, w.r.t. curvature κ.

Generalizing the previous approach, we compute paths globally minimizing various curvature dependent energies.

Reeds-Shepp forward

$\sqrt{1+\kappa^2}$

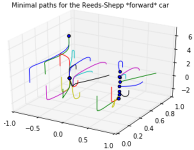

Euler-Mumford

$1+\kappa^2$

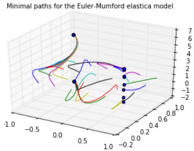

Dubins

$1+\infty_{\kappa>1}$

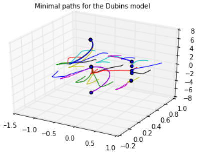

Figure: Backtracked geodesics,

Curvature penalized planar paths

The Reeds-Shepp model penalizes path curvature, but it:

- Allows for cusps (shift into reverse gear).
- Has specific cost dependency $\sqrt{1+\kappa^2}$, w.r.t. curvature κ.

Generalizing the previous approach, we compute paths globally minimizing various curvature dependent energies.

Reeds-Shepp forward	Euler-Mumford	Dubins
$\sqrt{1+\kappa^2}$	$1+\kappa^2$	$1+\infty_{\kappa>1}$

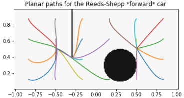

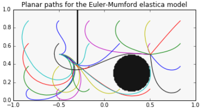

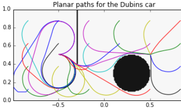

Figure: Backtracked geodesics, projected onto $\mathbb{R}^2$.

Computation of threatening trajectories, and optimization of a surveillance system. With J. Dreo.

- An adversary starts at •, then visits •, finally returns to •

Dubins car

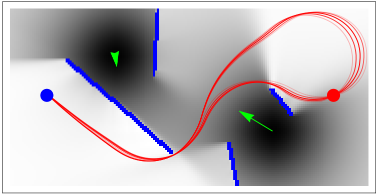

Dubins car

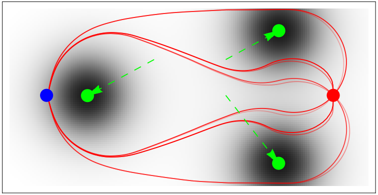

- Related work by Barbaresco, Strode.

Computation of threatening trajectories, and optimization of a surveillance system. With J. Dreo.

- An adversary starts at •, then visits •, finally returns to •
- His turning radius is bounded. *Admissible paths* Γ.

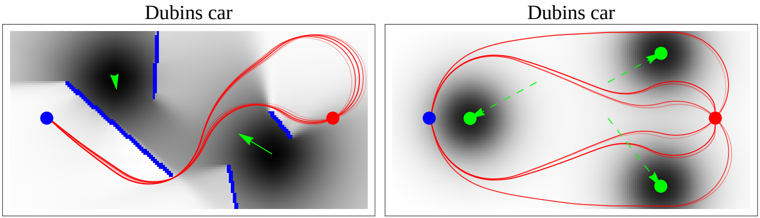

- Related work by Barbaresco, Strode.

Computation of threatening trajectories, and optimization of a surveillance system. With J. Dreo.

- An adversary starts at •, then visits •, finally returns to •
- His turning radius is bounded. *Admissible paths* Γ.
- Probability of detection depends on the distance and orientation relative to the sensors. *Cost function* $c_\lambda(x, n)$.

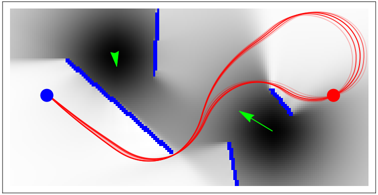

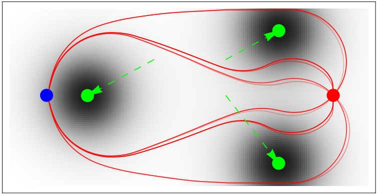

- Related work by Barbaresco, Strode.

Computation of threatening trajectories, and optimization of a surveillance system. With J. Dreo.

- An adversary starts at •, then visits •, finally returns to •
- His turning radius is bounded. *Admissible paths* Γ.
- Probability of detection depends on the distance and orientation relative to the sensors. *Cost function* $c_\lambda(x, n)$.
- Goal: optimize the sensor configuration $\lambda \in \Lambda$.

$$\max_{\lambda \in \Lambda} \min_{\gamma \in \Gamma} \int_0^{L(\gamma)} c_\lambda(\gamma(s), \gamma'(s)) \, \mathrm{d}s.$$

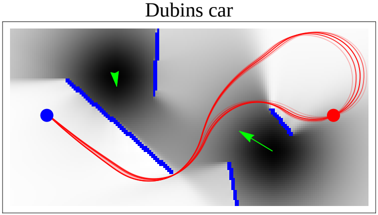

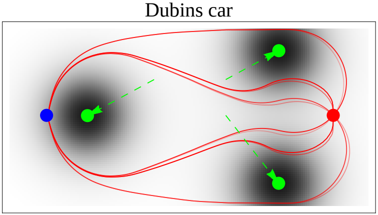

- Related work by Barbaresco, Strode.

Introduction: anisotropy and cartesian grids

Problems addressed

Finslerian eikonal equations, and the Stern-Brocot tree

Semi-Lagrangian schemes

Adaptive stencil refinement

Application to image segmentation

Riemannian eikonal equations, and Voronoi's reduction

Monotone and causal schemes

Grid-adapted tensor decomposition

Global optimization of curvature dependent energies

The Reeds-Shepp models

Euler-Mumford elastica curves, and others

Conclusion

Thanks for your attention.

- Cartesian grids, which are natural for numerous applications, are not incompatible with anisotropic pbs.

Numerical codes, demo notebooks, available at
`github.com/mirebeau/`

Thanks for your attention.

- Cartesian grids, which are natural for numerous applications, are not incompatible with anisotropic pbs.
- The tools of lattice geometry allow to build fast, robust, and accurate, adaptive numerical schemes.

Numerical codes, demo notebooks, available at
`github.com/mirebeau/`

Thanks for your attention.

- Cartesian grids, which are natural for numerous applications, are not incompatible with anisotropic pbs.
- The tools of lattice geometry allow to build fast, robust, and accurate, adaptive numerical schemes.
- Handling (strongly) anisotropic PDEs allows to address new models and applications.

Numerical codes, demo notebooks, available at
`github.com/mirebeau/`

References

[A1] M. Efficient fast marching with Finsler metrics. Numerische Mathematik, vol. 126, no. 3, pp. 515-557, 2013.

[A2] Jérôme Fehrenbach and M. Sparse Non-negative Stencils for Anisotropic Diffusion. Journal of Mathematical Imaging and Vision, vol. 49, no. 1, pp. 123-147, 2014.

[A3] M. Anisotropic Fast-Marching on cartesian grids using Lattice Basis Reduction. SIAM Journal on Numerical Analysis, vol. 52, no. 4, pp. 1573-1599, Jan. 2014.

[A4] Jérémy Bleyer, Guillaume Carlier, Vincent Duval, M, and Gabriel Peyré. A Γ-Convergence Result for the Upper Bound Limit Analysis of Plates. ESAIM: Mathematical Modelling and Numerical Analysis (M2AN), vol. 50, no. 1, pp. 215-235, 2016.

[A5] Jean-David Benamou, Francis Collino, and M. Monotone and Consistent discretization of the Monge-Ampere operator. Mathematics of Computation, vol. 85, no. 302, pp. 2743-2775, 2016.

[A6] M. Discretization of the 3D Monge-Ampere operator, between Wide Stencils and Power Diagrams. Mathematical Modeling and Numerical Analysis (M2AN), vol. 49, no. 5, pp. 1511-1523, 2015.

[A7] M. Adaptive, Anisotropic and Hierarchical Cones of Convex functions. Numerische Mathematik, vol. 132, no. 4, pp. 807-853, 2016.

References (continued)

[A8] Quentin Merigot and M. Minimal geodesics along volume preserving maps, through semi-discrete optimal transport, SIAM journal on Numerical Analysis, vol. 54, no. 6, pp. 3465-3492, 2016.

[A9] M. Minimal Stencils for Monotony or Causality Preserving Discretizations of Anisotropic PDEs, SIAM journal on Numerical Analysis, vol. 54, no. 3, pp. 1582-1611, 2016.

[A10] Da Chen, M, and Laurent Cohen, Vessel Tree Extraction using Radius-Lifted Keypoints Searching Scheme and Anisotropic Fast Marching Method, Journal of Algorithms and Computational Technology, vol. 10, no. 4, pp. 224-234, Jul. 2016.

[A11] Da Chen, M, and Laurent Cohen, Global Minimum For A Finsler Elastic Minimal Path Approach, International Journal of Compter Vision, vol. 122, no. 3, pp. 458-483, 2017.

[A12] Remco Duits, Stephan P.L. Meesters, M, Jorg M. Portegies, Optimal Paths for Variants of the 2D and 3D Reeds-Shepp Car with Applications in Image Analysis, Journal of Mathematical Imaging and Vision, 2018

[A13] M, Fast Marching Methods for Curvature Penalized Shortest Paths, Journal of Mathematical Imaging and Vision, 2018

[A14] M, Anisotropic fast-marching on cartesian grids using Voronoi's first reduction of quadratic forms, (submitted) 2018

Peer reviewed conference proceedings

[P1] Da Chen, Laurent D. Cohen, and M, Vessel Extraction Using Anisotropic Minimal Paths and Path Score, IEEE International Conference on Image Processing (ICIP), pp. 1570-1574, 2014.

[P2] Gonzalo Sanguinetti, Erik Bekkers, Remco Duits, Michiel Janssen, Alexey Mashtakov, and M, Sub-Riemannian Fast Marching in SE(2), Iberoamerican Congress on Pattern Recognition (CIARP), vol. 9423, no. 44, pp. 366-374, 2015.

[P3] Da Chen, M, and Laurent D. Cohen, Global Minimum for Curvature Penalized Minimal Path Method, British Machine Vision Conference (BMVC), pp 81-86, 2015.

[P4] Da Chen, M, and Laurent D. Cohen, A New Finsler Minimal Path Model with Curvature Penalization for Image Segmentation and Closed Contour Detection, IEEE Conference on Computer Vision and Pattern Recognition (CVPR), pp. 355-363, Jun. 2016.

[P5] Da Chen, M, and Laurent D. Cohen, Finsler Geodesic Evolution Model for Region based Active Contours, British Machine Vision Conference (BMVC), 2016.

[P6] M, Johann Dreo, Automatic differentiation of non-holonomic fast marching for computing most threatening trajectories under sensors surveillance, Geometric Science of Information (GSI), 2017

Introduction

Panorama

Finslerian eikonal

Semi-Lagrangian schemes

Adaptive stencil refinement

Image segmentation

Riemannian eikonal

Monotony and causality

Grid-adapted tensor decomposition

Curvature penalization

Reeds-Shepp

Other models

Conclusion

Reproducible research papers, with C++ codes

[R1] M, Jérôme Fehrenbach, Laurent Risser, and Shaza Tobji. Anisotropic Diffusion in ITK. The Insight Journal, 2015.

[R2] M. Anisotropic Fast-Marching in ITK. The Insight Journal, 2015.

[R3] M, Jorg Portegies. Hamiltonian Fast Marching. A numerical solver for anisotropic and non-holonomic eikonal PDEs. 2018 (Submitted)

The Reeds-Shepp model in the visual system.

- Neurons of the first layer V1 of the visual cortex react to stimuli at a specific position x and orientation $\theta \in [0, \pi]$.

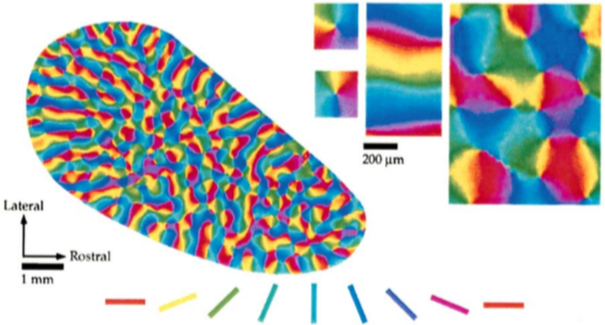

Figure: Pinwheel structure of V1. Orientations coded by color.

The Reeds-Shepp model in the visual system.

- Neurons of the first layer V1 of the visual cortex react to stimuli at a specific position x and orientation $\theta \in [0, \pi]$.
- *Short range connectivity (marked by biocytin's diffusion) is isotropic, while long-range connectivity is anisotropic and limited to iso-orientation domains.* Bosking et al.

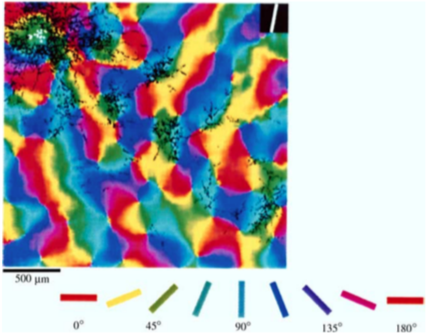

Figure: Pinwheel structure of V1. Orientations coded by color.

The Reeds-Shepp model in the visual system.

- Neurons of the first layer V1 of the visual cortex react to stimuli at a specific position x and orientation $\theta \in [0, \pi]$.
- *Short range connectivity (marked by biocytin's diffusion) is isotropic, while long-range connectivity is anisotropic and limited to iso-orientation domains.* Bosking et al.
- Petitot, Citti, Sarti, connect with the Reeds-Shepp model.

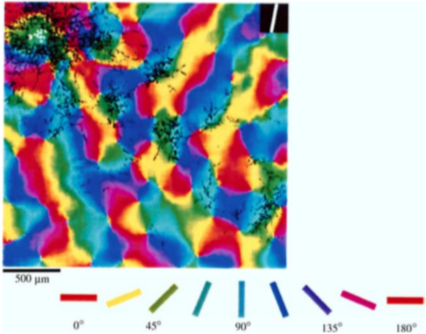

Figure: Pinwheel structure of V1. Orientations coded by color.

Poggendorff's visual illusions

According to Franceschiello et al, the visual system infers, between the endpoints of curves, a connection that:

- Has the correct tangents.
- Minimizes the Reeds-Shepp sub-Riemannian length.

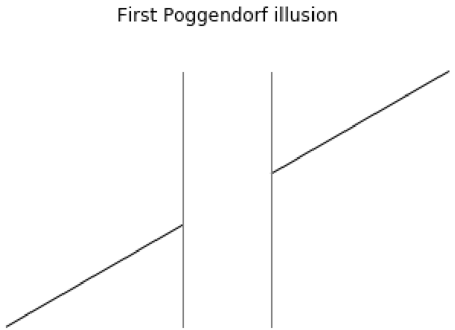

Figure: First Poggendorff illusion (perceived misalignment of lines), and its interpretation based on the Reeds-Shepp model.

Poggendorff's visual illusions

According to Franceschiello et al, the visual system infers, between the endpoints of curves, a connection that:

- Has the correct tangents.
- Minimizes the Reeds-Shepp sub-Riemannian length.

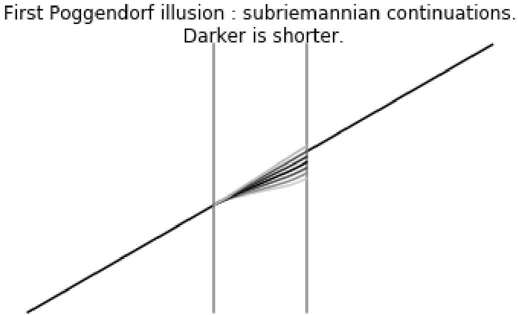

Figure: First Poggendorff illusion (perceived misalignment of lines), and its interpretation based on the Reeds-Shepp model.

Poggendorff's visual illusions

According to Franceschiello et al, the visual system infers, between the endpoints of curves, a connection that:

- Has the correct tangents.
- Minimizes the Reeds-Shepp sub-Riemannian length.

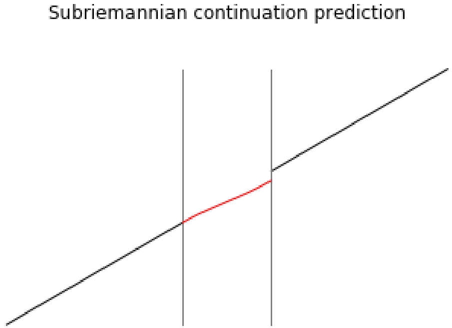

Figure: First Poggendorff illusion (perceived misalignment of lines), and its interpretation based on the Reeds-Shepp model.

Poggendorff's visual illusions

According to Franceschiello et al, the visual system infers, between the endpoints of curves, a connection that:

- Has the correct tangents.
- Minimizes the Reeds-Shepp sub-Riemannian length.

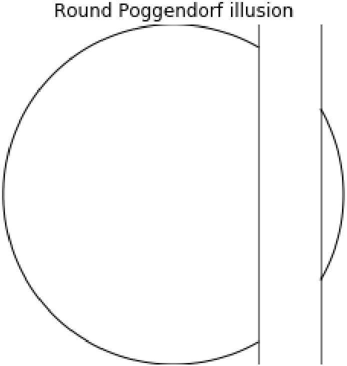

Figure: Second Poggendorf illusion (perceived misalignment of circle arcs), and its interpretation based on the Reeds-Shepp model.

Poggendorff's visual illusions

According to Franceschiello et al, the visual system infers, between the endpoints of curves, a connection that:

- Has the correct tangents.
- Minimizes the Reeds-Shepp sub-Riemannian length.

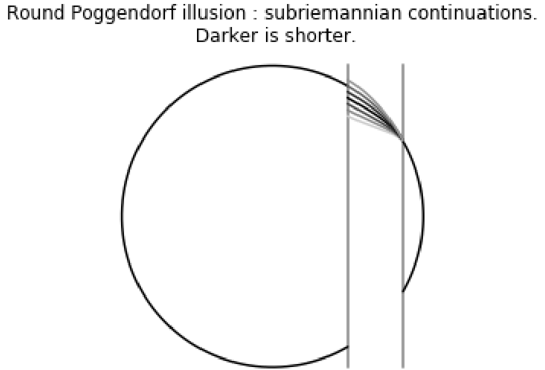

Figure: Second Poggendorf illusion (perceived misalignment of circle arcs), and its interpretation based on the Reeds-Shepp model.

Poggendorff's visual illusions

According to Franceschiello et al, the visual system infers, between the endpoints of curves, a connection that:

- Has the correct tangents.
- Minimizes the Reeds-Shepp sub-Riemannian length.

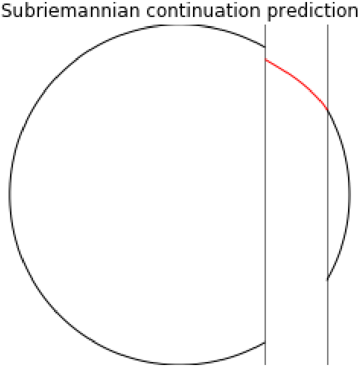

Figure: Second Poggendorf illusion (perceived misalignment of circle arcs), and its interpretation based on the Reeds-Shepp model.